Article

Cell Reports

Impaired Mitochondrial Dynamics and Mitophagy in Neuronal Models of Tuberous Sclerosis Complex

Graphical Abstract

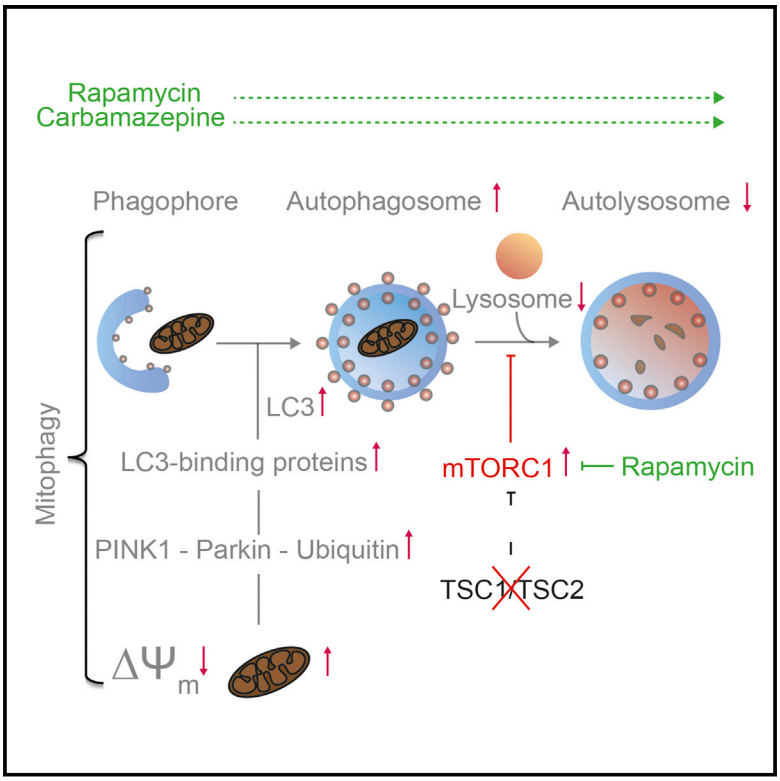

Authors

Darius Ebrahimi-Fakhari, Afshin Saffari, Lara Wahlster, ..., Min-Joon Han, Franck Polleux, Mustafa Sahin

Correspondence

mustafa.sahin@childrens.harvard.edu

In Brief

Ebrahimi-Fakhari et al. show that mitochondrial dynamics and mitophagy are impaired in neuronal models of tuberous sclerosis complex. Axonal transport, turnover, and presynaptic capturing of mitochondria are compromised. Enhancing autophagic flux through mTORC1-dependent and -independent mechanisms restores mitochondrial homeostasis.

Highlights

- Mitochondria, some of which are dysfunctional, accumulate in *Tsc2*-deficient neurons
- Axonal mitochondria, including those captured at presynaptic sites, are depleted
- Spatiotemporal dynamics of axonal mitophagy and global mitophagic flux are impaired
- Enhancing mTOR-dependent and -independent autophagy restores mitochondrial turnover

Ebrahimi-Fakhari et al., 2016, Cell Reports *17*, 1053–1070
October 18, 2016
http://dx.doi.org/10.1016/j.celrep.2016.09.054

Cell Reports
Article

Impaired Mitochondrial Dynamics and Mitophagy in Neuronal Models of Tuberous Sclerosis Complex

Darius Ebrahimi-Fakhari,[1,2,6] Afshin Saffari,[1,2,6] Lara Wahlster,[2,3] Alessia Di Nardo,[1] Daria Turner,[1] Tommy L. Lewis, Jr.,[4] Christopher Conrad,[5] Jonathan M. Rothberg,[5] Jonathan O. Lipton,[1] Stefan Kölker,[2] Georg F. Hoffmann,[2] Min-Joon Han,[1] Franck Polleux,[4] and Mustafa Sahin[1,7,*]

[1]The F.M. Kirby Neurobiology Center, Translational Neuroscience Center, Department of Neurology, Boston Children's Hospital, Harvard Medical School, Boston, MA 02115, USA
[2]Division of Pediatric Neurology and Metabolic Medicine, Center for Child and Adolescent Medicine, University Hospital Heidelberg, 69120 Heidelberg, Germany
[3]Division of Hematology and Oncology, Stem Cell Program, Boston Children's Hospital, Harvard Medical School, Boston, MA 02115, USA
[4]Department of Neuroscience, Zuckerman Mind Brain Behavior Institute and Kavli Institute for Brain Science, Columbia University, New York, NY 10027, USA
[5]LAM Therapeutics, Guilford, CT 06437, USA
[6]Co-first author
[7]Lead Contact
*Correspondence: mustafa.sahin@childrens.harvard.edu
http://dx.doi.org/10.1016/j.celrep.2016.09.054

SUMMARY

Tuberous sclerosis complex (TSC) is a neurodevelopmental disease caused by *TSC1* or *TSC2* mutations and subsequent activation of the mTORC1 kinase. Upon mTORC1 activation, anabolic metabolism, which requires mitochondria, is induced, yet at the same time the principal pathway for mitochondrial turnover, autophagy, is compromised. How mTORC1 activation impacts mitochondrial turnover in neurons remains unknown. Here, we demonstrate impaired mitochondrial homeostasis in neuronal in vitro and in vivo models of TSC. We find that *Tsc1/2*-deficient neurons accumulate mitochondria in cell bodies, but are depleted of axonal mitochondria, including those supporting presynaptic sites. Axonal and global mitophagy of damaged mitochondria is impaired, suggesting that decreased turnover may act upstream of impaired mitochondrial metabolism. Importantly, blocking mTORC1 or inducing mTOR-independent autophagy restores mitochondrial homeostasis. Our study clarifies the complex relationship between the TSC-mTORC1 pathway, autophagy, and mitophagy, and defines mitochondrial homeostasis as a therapeutic target for TSC and related diseases.

INTRODUCTION

Tuberous sclerosis complex (TSC) is a neurodevelopmental disease caused by loss-of-function mutations in the *TSC1* or *TSC2* gene and subsequent activation of the mTORC1 kinase (DiMario et al., 2015; Lipton and Sahin, 2014). Although mTORC1 inhibitors have emerged as a therapy for certain disease manifestations, their impact on complex neurological manifestations remains uncertain (https://clinicaltrials.gov/: NCT01289912, NCT01730209, and NCT01954693). It is imperative to understand the molecular mechanisms that result from loss-of-function mutations in *TSC1/2* and that may promote intellectual disability, seizures, or autism spectrum disorder in TSC.

Despite the fact that many TSC/mTORC1-related functions have been extensively studied in non-neuronal cell types (Albert and Hall, 2015), many remain unexplored in neuronal models of TSC. Constitutive activation of mTORC1 has been shown to promote anabolic metabolism, while simultaneously repressing catabolic processes such as autophagy. Mitochondria play a crucial role in supporting anabolic metabolism, yet at the same time, their function, maintenance, and turnover are tightly regulated by autophagic flux. A central question thus remains how *TSC1/2* deficiency impacts mitochondrial homeostasis in neurons.

In neurons, mitochondria form a highly dynamic reticular network and undergo constant remodeling and turnover. To support local demands for mitochondrial ATP supply and calcium buffering capacity, mitochondria are transported along microtubule tracks to remote axonal regions (Maday et al., 2014), and conversely dysfunctional mitochondria are returned to the cell body for degradation (Cai et al., 2012). Maintenance of a functional population of mitochondria is ensured through effective autophagic degradation of aged and damaged mitochondria, a process that has been termed mitophagy (Pickrell and Youle, 2015).

Neuropathological studies of mouse models of TSC and TSC patients document impaired autophagic flux, and an accumulation of organelles, including mitochondria (Di Nardo et al., 2014; Goto et al., 2011; McMahon et al., 2012; Tang et al., 2014; Yasin et al., 2013). The functional importance of the latter is corroborated by increased levels of oxidative stress in neuronal models of TSC (Di Nardo et al., 2009; Tsai et al., 2012). Despite these striking observations, however, relatively little is known about

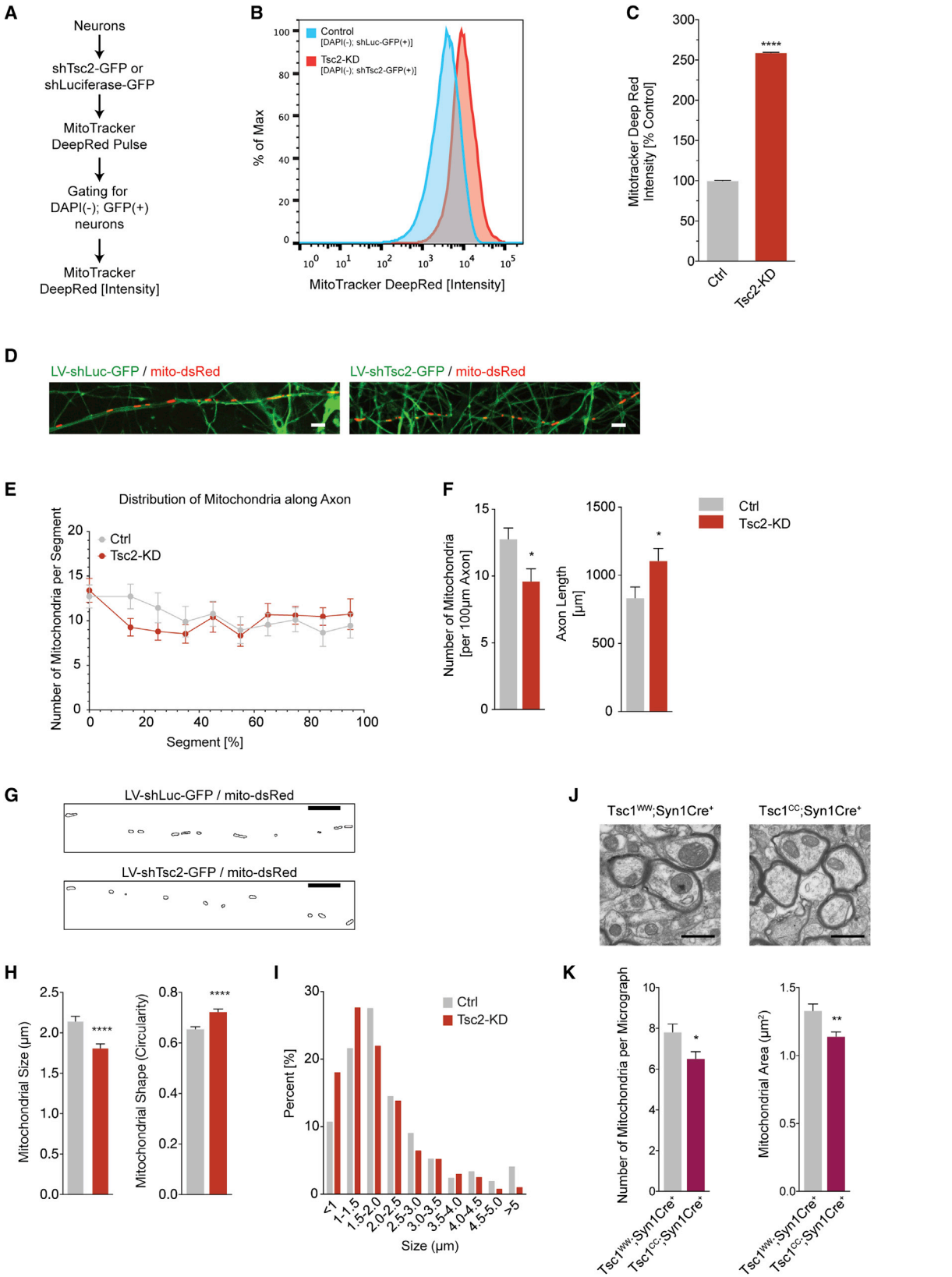

(legend on next page)

the impact of TSC/mTORC1 on the turnover of neuronal mitochondria.

Here, we investigate mitochondrial dynamics, metabolism, and turnover in neuronal in vitro and in vivo models of TSC. We find that *Tsc1/2*-deficient neurons progressively accumulate mitochondria in cell bodies but are depleted of functional mitochondria in axons, including those that support presynaptic sites. The dynamics of mitophagy are impaired both locally in axons and globally across the neuron. Localizing the defect to the late stages of the mitophagy pathway, we find that autophagosome turnover is impaired. Finally, we find that either blocking mTORC1 or inducing mTOR-independent autophagy can reverse changes in mitochondrial homeostasis seen in *Tsc1/2*-deficient neurons. Collectively, these results provide evidence for a previously unappreciated role of impaired neuronal mitophagy in TSC. Addressing the role of mTORC1 in mitochondrial turnover holds the promise for a better understanding of TSC and the identification of therapeutic targets.

RESULTS

Mitochondria Accumulate in *Tsc2*-Deficient Neurons but Are Depleted from Axons

We hypothesized that *Tsc2* deficiency induced mTORC1 activation might impact mitochondrial homeostasis. To address this, we employed a flow cytometry-based assay (Mauro-Lizcano et al., 2015) to quantitate mitochondrial content (Figure 1A). We found that *Tsc2*-deficient neurons, with constitutive and significant mTORC1 activation (Figure S1A; Choi et al., 2008), accumulate mitochondria and show an increase in mitochondrial mass to ~2.5-fold the level of controls (Figures 1B and 1C). This increase progresses even further as neurons mature in culture (Figure S1B), cannot be explained by an increase in cell size alone (Figure S1C), and mimics that observed in giant cells of *Tsc1^{cc};Nes-rtTA^{+};TetOp-Cre^{+}* (E16 doxy) mice (Goto et al., 2011). Increased mitochondrial mass can result from an increase in mitochondrial biogenesis, a decrease in mitochondrial turnover, or both. Importantly, the transcription of critical mitochondrial biogenesis genes is not upregulated in *Tsc2*-deficient neurons (Figure S1D). In fact, we observed no change in *Pgc1α* expression and reduced expression levels of the *Nrf1* and *mtTFA* in *Tsc2*-knockdown neurons (Figure S1D). Levels of the mtDNA-encoded *COX-II* were also reduced, whereas levels of the nuclear DNA-encoded *COX-IV* were unchanged (Figure S1D). These findings contrast with observations in non-neuronal cells (Cunningham et al., 2007; Morita et al., 2013) and argue that mitochondrial biogenesis is not increased in *Tsc2*-deficient neurons.

To examine the distribution and dynamics of mitochondria, we employed confocal live-cell imaging. Mitochondria in both conditions form a dense network in the cell body, whereas they sparsely populate axons (Figures 1D, 1E, and S1E). Consistent with previous reports, we found that axon outgrowth is accelerated in *Tsc2*-deficient neurons with an overall increase in axon length (Figure 1F) and multiple axons frequently occurring (Choi et al., 2008). Quantifying mitochondria along axons (Figure 1E), we found that *Tsc2*-deficient axons contain fewer mitochondria per 100 μm (Figure 1F), although their relative distribution follows a similar pattern to that of controls, with more mitochondria in the proximal axon (Figure 1E). This finding suggests that *Tsc2*-deficient axons are relatively depleted of mitochondria with the remaining mitochondria redistributing to cover the full length of the axon.

Mitochondrial morphology changes are intimately linked to mitochondrial dynamics and thus can serve as a surrogate marker to screen for underlying abnormalities (Pernas and Scorrano, 2016). Small and circular mitochondria often indicate mitochondrial membrane depolarization and increased production of reactive oxygen species. Axonal mitochondria in controls were mostly tubular in shape and variable in size (Figures 1G–1I). In contrast, *Tsc2*-deficient axons contained mitochondria that were significantly smaller and displayed a more circular shape, signifying mitochondrial fragmentation (Figures 1G and 1H). The relative distribution of mitochondrial size revealed a left shift in *Tsc2*-deficient neurons, indicating a greater proportion of small, fragmented mitochondria (Figure 1I). Reintroducing *TSC2* was able to reverse changes in the morphology and number of axonal mitochondria, suggesting that these are indeed a consequence of disturbed TSC-mTORC1 signaling (Figure S1F). Further corroborating these findings in vivo using electron microscopy, we found that commissural axons of the corpus callosum of *Tsc1^{cc};Syn1Cre^{+}* mice (Meikle et al., 2007) showed both a reduced number of mitochondria and a decreased organelle size (Figures 1J and 1K).

In summary, *Tsc2*-deficient neurons accumulate mitochondria in their cell body but are relatively depleted of axonal mitochondria with the remaining mitochondria showing an abnormal morphology indicative of disrupted mitochondrial dynamics.

Figure 1. *Tsc2*-Deficient Neurons Accumulate Mitochondria in Their Cell Bodies but Are Depleted of Axonal Mitochondria

(A–C) Flow cytometry-based quantification of mitochondrial content using MTDR in cortical neurons (DIV11). Note that this assay primarily quantifies the mitochondrial content in cell bodies since neurites may be lost during sample preparation (n = 9 × 10^6 recorded events per condition from nine independent samples).

(D) Live-cell confocal imaging of individual mitochondria in single axons of hippocampal neurons transduced with shLuc-GFP or shTsc2-GFP (DIV7/8). Scale bar, 5 μm.

(E) Distribution of mitochondria along the full length of axons in hippocampal neurons (DIV7/8, n = 40 axons per condition from 8–10 experiments).

(F) Number of mitochondria per 100 μm of axon and the average length of axons in hippocampal neurons (DIV7/8, n = 40 axons per condition from 8–10 experiments).

(G–I) Quantitative assessment of mitochondrial morphology (circularity and Feret's diameter) in axons of hippocampal neurons (DIV7/8, n > 400 mitochondria per condition from 8–10 experiments). Scale bar, 10 μm.

(J and K) Transmission electron microscopy of callosal projection axons from *Tsc1^{CC};Syn1Cre^{+}* (n = 2) and *Tsc1^{WW};Syn1Cre^{+}* littermates (n = 3). Graphs show the number of mitochondria per micrograph and the average mitochondrial area (n > 450 mitochondria per condition). Scale bar, 1 μm.

Luc, Luciferase; *p < 0.05, **p < 0.01, ***p < 0.001, ****p < 0.0001. See also Figure S1.

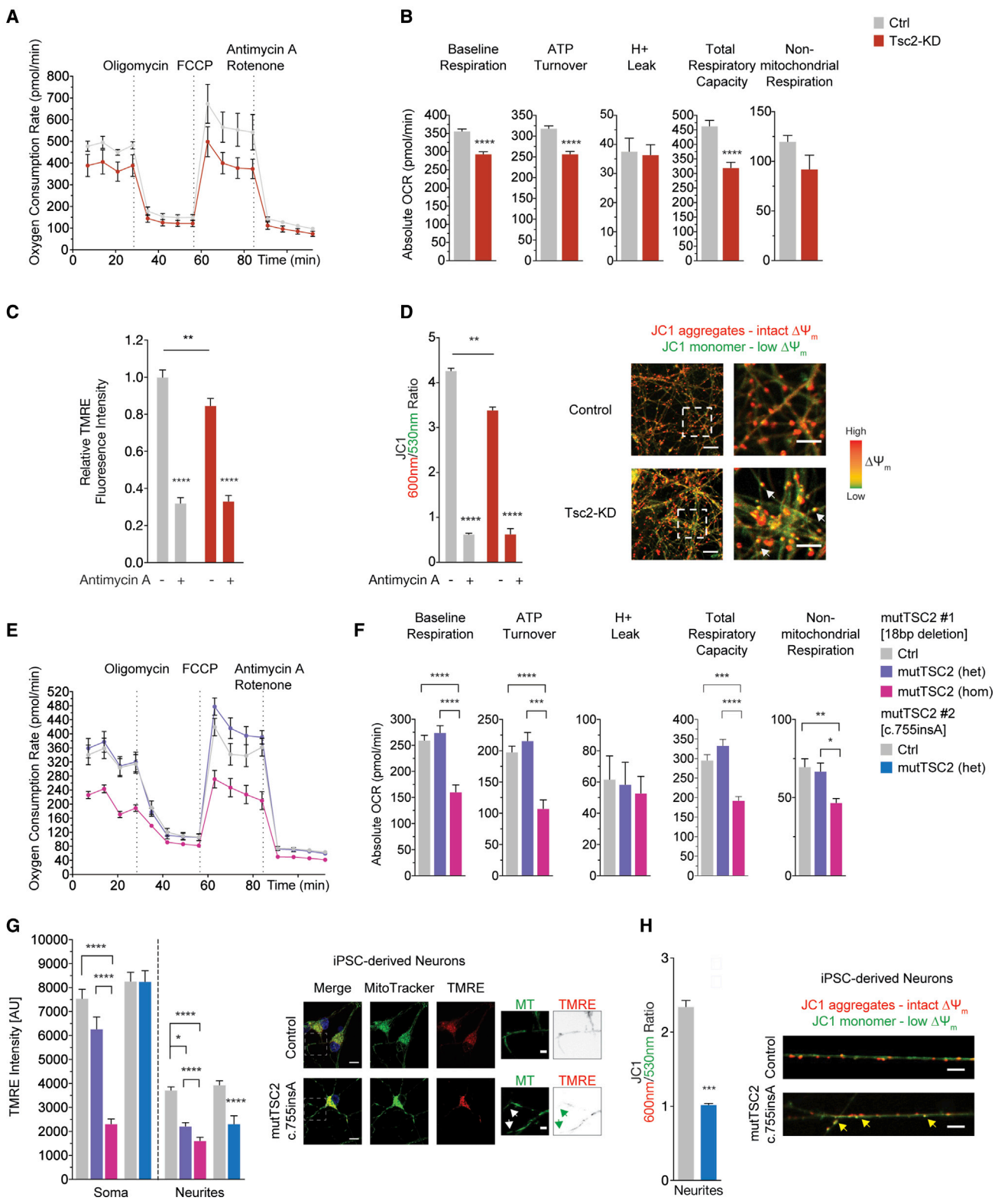

Figure 2. Mitochondrial respiration Is Impaired and Mitochondrial Membrane Potential, $\Delta\Psi_m$, Is Diminished in *Tsc2*-Deficient Neurons and Neurites of Human iPSC-Derived Cortical Neurons from TSC Patients

(A and B) Mitochondrial oxygen consumption rates in hippocampal neurons (DIV8) measured using the Seahorse XF Extracellular Flux 96 analyzer. Graphs show different domains of mitochondrial function and non-mitochondrial respiration (n = 10 measurements per condition).

(legend continued on next page)

Mitochondrial Respiration Is Impaired and Mitochondrial Membrane Potential, $\Delta\Psi_m$, Is Diminished in *Tsc2*-Deficient Neurons and Mutant *TSC2* Induced Pluripotent Stem Cell-Derived Neurons

To investigate the effect of *Tsc2* deficiency on mitochondrial function, we measured oxygen consumption rates and the functional parameters that can be derived from it (Figure S2A). In *Tsc2*-deficient neurons, we found impaired mitochondrial bioenergetics, evidenced by a reduction in baseline respiration, ATP turnover, and total respiratory capacity (Figures 2A and 2B). This effect was specific to mitochondrial metabolism as non-mitochondrial respiration and proton leak did not change (Figure 2B).

An intact mitochondrial membrane potential ($\Delta\Psi_m$) is a key requisite for effective oxidative phosphorylation. To approximate $\Delta\Psi_m$, we used tetramethylrhodamine ethyl ester (TMRE), a $\Delta\Psi_m$-dependent dye. In *Tsc2*-deficient neurons, TMRE signal was reduced (Figure 2C), reflecting a subset of mitochondria that exhibit a decreased $\Delta\Psi_m$. To localize mitochondria with a diminished $\Delta\Psi_m$, we employed the ratiometric $\Delta\Psi_m$ indicator, JC-1 (Figure 2D). In control neurons, the vast majority of mitochondria show a high 600/530-nm ratio, indicating an intact $\Delta\Psi_m$ (Figure 2D). In *Tsc2*-deficient neurons, we found a significant shift toward a lower 600/530-nm ratio (Figure 2D), arguing for a reduced electrochemical status in a significant subset. Importantly, these mitochondria with diminished $\Delta\Psi_m$ were readily detectable in neurites of *Tsc2*-deficient neurons (Figure 2D, white arrows). Expression analyses of electron transport chain subunits revealed an increase of complex I (subunit NDUFB8), a major site for reactive oxygen species production (Murphy, 2009), and a decrease of complex II (subunit 30 kDa) in *Tsc2*-deficient neurons (Figure S2B).

To test whether disease-specific mutations in patient-derived cells share similar changes in mitochondrial function, we generated induced pluripotent stem cell (iPSC)-derived cortical neurons (Zhang et al., 2013) from individuals with TSC and controls (Table S1). We discovered that patient-derived neurons with a heterozygous *TSC2* mutation did not display detectable deficits in mitochondrial respiration (Figures 2E and 2F). However, upon introduction of a second loss-of-function mutation using transcription activator-like effector nucleases (TALEN), we found a marked reduction in mitochondrial function similar to that in rat *Tsc2*-KD cortical neurons (Figures 2E and 2F). Next, we pulse-labeled mitochondria with TMRE and MTDR ($\Delta\Psi_m$ independent) and quantified the TMRE intensity in the soma and neurites (Figure 2G). TMRE signal in the soma was similar between $TSC2^{+/-}$ iPSC-derived neurons and controls, but reduced in homozygous mutants (Figure 2G). The TMRE signal in neurites was overall weaker than that in the soma, likely reflecting the high density of mitochondria in the latter (Figure 2G). Compared to controls, neurites of $TSC2^{+/-}$ and $TSC2^{-/-}$ iPSC-derived cortical neurons contained many mitochondria with a low TMRE fluorescence, although they retained their MitoTracker Deep Red (MTDR) signal (Figure 2G, arrows), suggesting an accumulation of depolarized mitochondria. This was confirmed using the JC1 assay (Figure 2H, arrows). Notably, we detected mTORC1 activation in $TSC2^{+/-}$ iPSC-derived neurons (M-J.H. and M.S., unpublished data), similar to recently published observations of mTORC1 hyperfunction in $TSC2^{+/-}$ human embryonic stem cell-derived neurons (Costa et al., 2016).

Taken together, these findings suggest that multiple domains of mitochondrial bioenergetics are compromised in both *Tsc2*-deficient rodent neurons and TSC patient-derived neurons in vitro.

Axonal Mitochondria in *Tsc2*-Deficient Neurons Are Shuttled to the Cell Body Leading to a Depletion of Presynaptic Mitochondria

Neurons are unique in their architecture with critical compartments, such as axons and synapses, located far from the cell body. In *Tsc2*-deficient neurons, we observed increased mitochondrial mass in the cell body but mitochondrial depletion from axons (Figures 1C and 1F), arguing for a redistribution of axonal mitochondria. To examine axonal transport in *Tsc2*-deficient neurons, we selected a mid-axonal segment, 500–800 μm from the cell body, to avoid regional differences in mitochondrial transport (Figures 3A and S3A; Movies S1 and S2). Consistent with previous reports in similar assays (Pekkurnaz et al., 2014; Wang and Schwarz, 2009), mitochondria in control neurons are stationary in ~80%–85% of the time and are moving bidirectionally ~15%–20% of the time (Figures 3A and 3B). Strikingly, mitochondria in *Tsc2*-deficient neurons spend less time in a stationary position and instead display markedly enhanced retrograde transport (Figures 3A and 3B).

Axonal mitochondria undergo dynamic transport, and motile mitochondria often pause and move again in response to physiological changes. We found that mitochondria in *Tsc2*-deficient axons exhibited more stops and more frequent changes in direction (Figure 3C). Examining the kymographic morphology, we discovered that a subset of mitochondria in *Tsc2*-deficient axons showed a peculiar oscillating movement pattern, moving back and forth without any significant net displacement (Figure 3A,

(C) TMRE staining in hippocampal neurons (DIV7/8). Healthy mitochondria with an intact $\Delta\Psi_m$ accumulate TMRE, thus displaying high TMRE fluorescence, whereas dysfunctional mitochondria show reduced TMRE signal. Antimycin A (40 μM, 1 hr), a complex III inhibitor, leads to a rapid breakdown of the $\Delta\Psi_m$, confirming dynamic assay properties (n = 8 measurements per condition).

(D) JC1 staining in hippocampal neurons (DIV7/8). JC-1 accumulates in mitochondria in a $\Delta\Psi_m$-dependent manner, where it exists as monomers at low concentrations (emission, 530 nm) and forms aggregates at higher concentrations (emission, 600 nm). Representative confocal images of mitochondria in neurites. Arrows denote mitochondria with low $\Delta\Psi_m$ (n = 6 experiments).

(E and F) Mitochondrial oxygen consumption rates in iPSC-derived cortical neurons from a TSC patient with a heterozygous *TSC2* mutation (mutTSC2 [het]); the same cell line with a second, engineered *TSC2* mutation leading to a complete loss of *TSC2* (mutTSC2 [hom]); and a healthy related donor (Ctrl) (summarized in Table S1). Graphs show different domains of mitochondrial function and non-mitochondrial respiration (n = 6 measurements per condition).

(G and H) TMRE and JC1 staining in iPSC-derived cortical neurons (summarized in Table S1). Arrows denote mitochondria with low $\Delta\Psi_m$ (TMRE: n > 35 cells per condition from 3 experiments; JC1: n > 85 mitochondria per condition from 3 experiments).

het, heterozygous; hom, homozygous; MT, MitoTracker. *p < 0.05, **p < 0.01, ***p < 0.001, ****p < 0.0001. See also Figure S2.

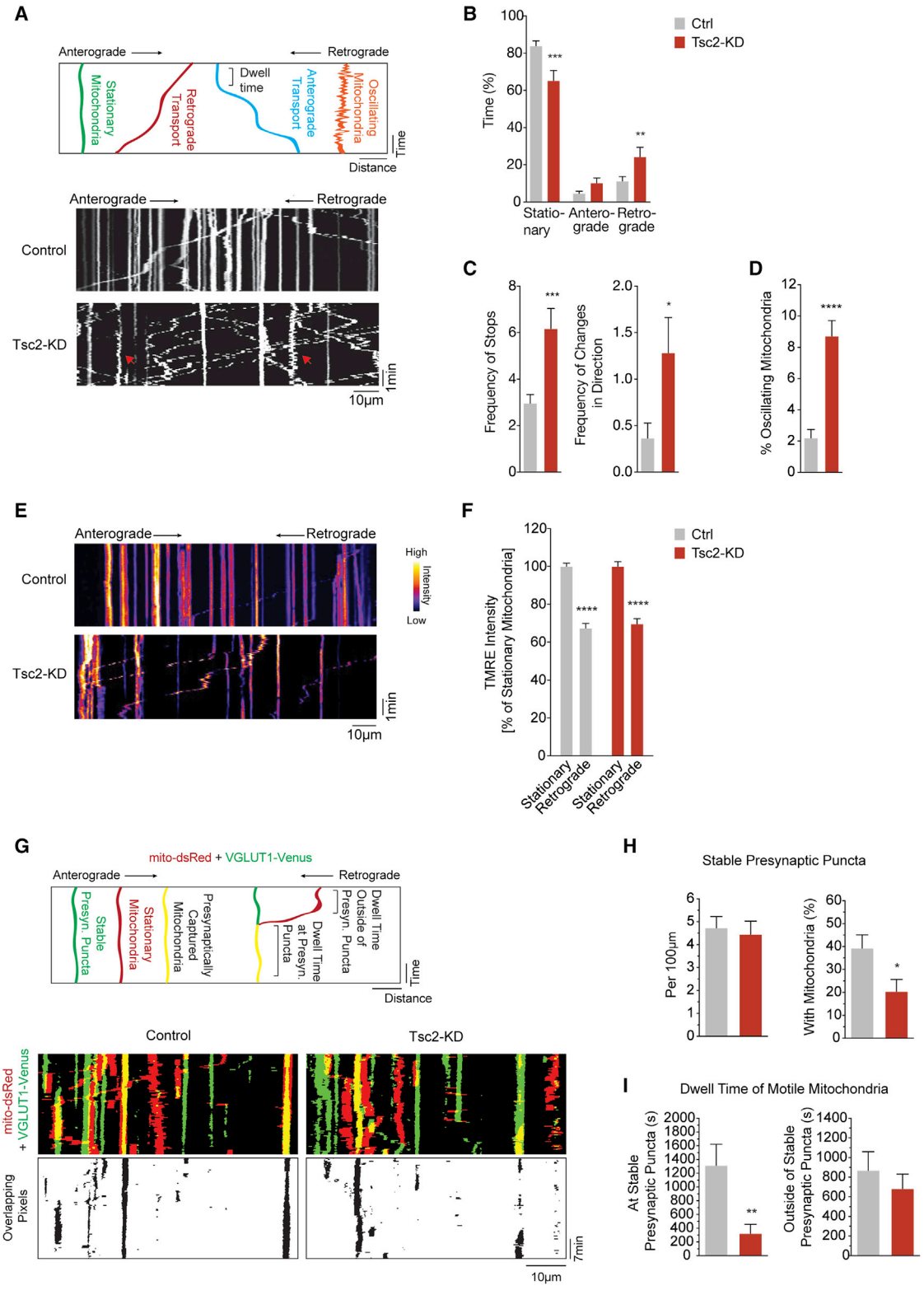

(legend on next page)

red arrows). Although ~2% of mitochondria in control neurons showed this pattern, this rate was increased to ~9% in *Tsc2*-deficient neurons (Figure 3D). A similar oscillating pattern has been recently reported in axonal mitochondria of PINK1 or Parkin overexpressing *Drosophila melanogaster* (Devireddy et al., 2015), potentially linking it to incipient mitophagy.

No change in the axonal transport pattern of other cargo, such as lysosomes, was observed, arguing that the effect of *Tsc2* deficiency on mitochondria is relatively specific (Figure S3B). Overexpression of the anchoring protein syntaphilin almost completely arrested mitochondrial transport, confirming that general mechanisms of axonal transport and anchoring are intact (Figure S3C).

Since we observed an accumulation of mitochondria with low $\Delta\Psi_m$ in *Tsc2*-deficient neurites, we hypothesized that these potentially damaged mitochondria might be successively returned to the cell body, as previously suggested (Cai et al., 2012). Indeed, mitochondria transported in the retrograde direction displayed a reduced TMRE fluorescence in both control and *Tsc2*-deficient axons (Figures 3E and 3F), indicating that dysfunctional mitochondria are preferentially returned to the cell body.

Stationary mitochondria are enriched at presynaptic sites where they supply ATP and buffer calcium, functions that are critical for synaptic vesicle release. Similarly, motile mitochondria passing through presynaptic boutons can dynamically influence synaptic transmission (Sun et al., 2013). We hypothesized that increased retrograde transport and depletion of axonal mitochondria in *Tsc2*-deficient neurons might influence the availability of mitochondria to synapses. To investigate the presynaptic capturing of mitochondria, we performed dual-channel time-lapse confocal microscopy in axons of neurons transfected with mito-DsRed and VGLUT1-Venus at days in vitro 7/8 (DIV7/8) (Figure 3G) and DIV14/15 (Figure S3D) as described previously (Courchet et al., 2013). *Tsc2* downregulation did not affect the density of stable VGLUT1-Venus puncta (Figure 3H). However, quantifying the number of stable presynaptic sites that contain stationary mitochondria, we discovered a ~50% reduction of mitochondria captured at presynaptic sites (Figure 3H). We also observed that motile mitochondria frequently dwell over stable VGLUT1 puncta in control axons (Figure 3I). In contrast, in *Tsc2*-deficient axons, we found a decrease in the time that motile mitochondria spend over stable VGLUT1-postive presynaptic sites, whereas the dwell time outside the presynaptic compartment did not differ from controls (Figure 3I). In more mature neurons at DIV14/15, most axonal mitochondria maintain a stationary position (Figure S3D). Looking at the number of stationary mitochondria captured at presynaptic sites, we found that mature *Tsc2*-deficient axons contained fewer synapses that are supported by local stationary mitochondria (Figure S3E). Hence, presynaptic capture of mitochondria is diminished in both developing and more mature *Tsc2*-deficient neurons in vitro.

Collectively, these experiments reveal enhanced retrograde transport of dysfunctional mitochondria as a potential mechanism that depletes axonal mitochondria in *Tsc2*-deficient neurons. Importantly, the availability of mitochondria to presynaptic sites is compromised arguing for insufficient mitochondrial capture.

Spatiotemporal Dynamics of Local Mitophagy Are Impaired in Axons of *Tsc2*-Deficient Neurons

The above experiments indicate alterations in mitochondrial mass, dynamics, and function that suggest impairment of mitochondrial turnover. Mitochondrial turnover via mitophagy occurs both locally in axons (Ashrafi et al., 2014) and in the soma (Cai et al., 2012). Might changes in mitophagy help explain decreased mitochondrial turnover? To address this question, we investigated both axonal mitophagy and global mitophagic flux.

To stimulate mitophagy in axons (Figure 4A), we employed treatment with antimycin A, which leads to a rapid loss of $\Delta\Psi_m$ (Figure S4A), thus allowing us to investigate mitophagic events in a time frame amenable to live-cell imaging without impairing axonal integrity (Ashrafi et al., 2014) (Figure S4B). Consistent with previous studies (Wang et al., 2011), we found that acute $\Delta\Psi_m$ depolarization renders most axonal mitochondria stationary (Figure S4C; Movie S3), and induces rapid fragmentation (Figures 4B and S4D), which may precede mitophagy. We approximated the rates of early mitophagy in axons by quantifying the percentage of Venus-LC3 puncta that co-localize with mitochondria following $\Delta\Psi_m$ depolarization (Klionsky et al., 2016). At baseline, Venus-LC3 is mostly cytosolic and only a small fraction of Venus-LC3 vesicles co-localize with mitochondria (Figures 4C and 4D). In response to $\Delta\Psi_m$ depolarization, however, we observed accumulation of Venus-LC3 on mitochondria with ~20% of mitochondria becoming coated with LC3 in control neurons (Figure 4D). In contrast, we observed a blunted mitophagic response in *Tsc2*-deficient neurons with

Figure 3. Axonal Mitochondria in *Tsc2*-Deficient Neurons Are Shuttled to the Cell Body and Presynaptic Capturing of Mitochondria Is Impaired

(A) Mitochondrial transport quantified through a standardized live-cell microscopy assay (see Figure S3A).

(B and C) Mitochondrial transport in the mid-axon of hippocampal neurons (DIV7/8). Graph shows the time that mitochondria spend in a stationary position, or moving in the retrograde or anterograde direction. The frequency of stops and changes in direction per 5-min recording is calculated (n > 25 axons per condition from 5–8 experiments).

(D) Percentage of axonal mitochondria with an oscillating movement pattern (n > 25 axons per condition from 5–8 experiments).

(E and F) TMRE staining in stationary mitochondria versus mitochondria transported in the retrograde direction (n > 10 axons per condition from 3 experiments).

(G) Quantitative assessment of mitochondrial capturing at presynaptic sites and representative examples (DIV7/8).

(H) Number of stable presynaptic puncta per 100-μm axon and the percentage of stable presynaptic puncta supported by stationary mitochondria in hippocampal neurons (DIV7/8, n = 14 axons per condition from 7 experiments).

(I) Average dwell time of motile mitochondria at and outside of stable presynaptic puncta in hippocampal neurons (DIV7/8, n = 14 axons per condition from 7 experiments).

*p < 0.05, **p < 0.01, ***p < 0.001, ****p < 0.0001. See also Figure S3.

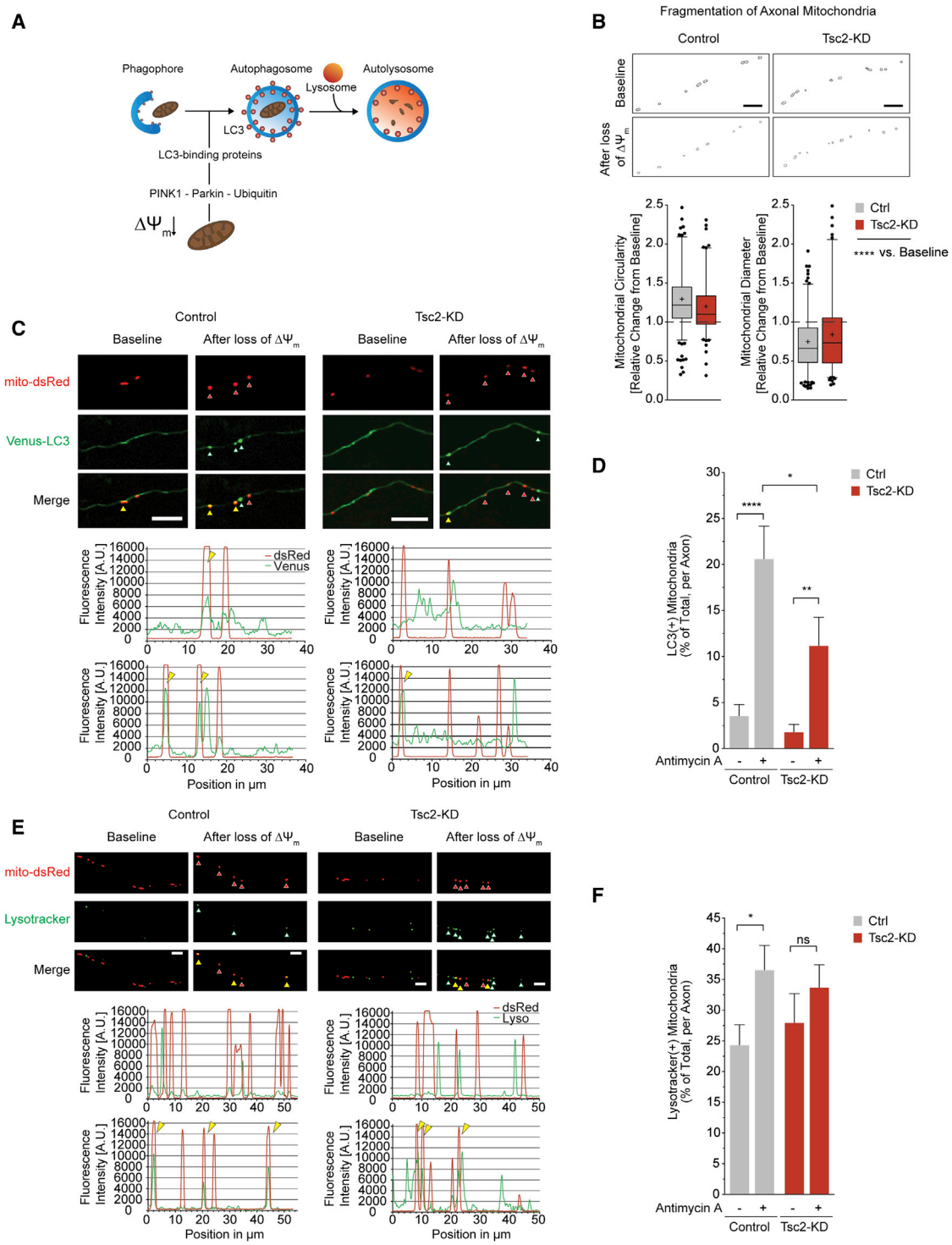

Figure 4. Spatiotemporal Dynamics of Axonal Mitophagy Are Impaired in *Tsc2*-Deficient Neurons

(A) Schematic showing the sequence of events during mitophagy.

(B) Morphology of axonal mitochondria before and after acute $\Delta\Psi_m$ depolarization with antimycin A (40 μM, n > 140 mitochondria per condition from 5 experiments). Scale bar, 5 μm.

(C and D) Recruitment of autophagosomes to axonal mitochondria following acute $\Delta\Psi_m$ depolarization with antimycin A (40 μM). Arrows denote mito-dsRed-labeled mitochondria (red), Venus-LC3-labeled autophagosomes (white), and their co-localization (yellow). Graph shows the maximal percentage of mitochondria co-localizing with autophagosomes in individual axons (n > 40 axons per condition from 12 experiments). Scale bar, 10 μm.

(legend continued on next page)

only a small proportion of mitochondria co-localizing with Venus-LC3 vesicles (Figure 4D). These data suggest that *Tsc2* deficiency results in impaired spatiotemporal dynamics of local mitophagy in axons.

Autophagic degradation of mitochondria is a multistep pathway (Figure 4A). To examine the late stages, we quantified the autophagic delivery of mitochondria to lysosomes. At baseline, we observed lysosomes in axons, a portion of which co-localized with mitochondria (Figures 4E and 4F). Following mitophagy induction, we found a significant increase in the co-localization of lysosomes with mitochondria in control neurons. In *Tsc2*-deficient neurons, however, we could not detect a similar increase (Figures 4E and 4F).

Taken together, these results reveal impaired recruitment of autophagosomes and lysosomes to damaged axonal mitochondria in *Tsc2*-deficient neurons, although some degree of early mitophagy is retained.

Global Mitophagic Flux Is Impaired in *Tsc2*-Deficient Neurons

Mitophagy has been well characterized in the cell body of neurons, where the majority of mature, acidic lysosomes reside (Johnson et al., 2016). To examine baseline steady-state levels of mitophagy, we purified mitochondria-enriched fractions from *Tsc2*-deficient neurons and controls as previously described (Figures 5A and S5A; Narendra et al., 2010). Levels of the autophagy markers LC3-II and p62 (Figures 5B and 5C) were robustly increased both in the cytosol and in mitochondria-enriched fractions from *Tsc2*-deficient neurons relative to controls, indicating an accumulation of autophagosomes and autophagy substrates. Measuring levels of PINK1 and Parkin, two proteins involved in mitophagy (Pickrell and Youle, 2015), we found that both were enriched in mitochondrial fractions of *Tsc2*-deficient neurons, potentially reflecting mitochondrial damage and early mitophagic events (Figures 5D and 5E).

The above experiments allow us to investigate the early steps of mitophagy but do not assess the net flux through the pathway. To investigate mitophagic flux, we employed flow cytometry (Figure 5F). We induced mitophagy by depolarizing mitochondria with a low dose of carbonyl cyanide *m*-chlorophenyl hydrazone (CCCP), a compound that dissipates the $\Delta\Psi_m$ (Mauro-Lizcano et al., 2015). Mitochondrial mass was determined by staining with the $\Delta\Psi_m$-independent mitochondrial dye MTDR (Figure 5F–5H). In control neurons, 24 hr of CCCP led to a reduction of ~10% of MTDR fluorescence relative to untreated cells (Figure 5G), indicating that depolarized mitochondria are degraded efficiently. As expected, co-treatment with saturating concentrations of bafilomycin A1, a compound that blocks autophagosome-lysosome fusion (Klionsky et al., 2016), prevented this decrease (Figure S5B). In *Tsc2*-deficient neurons treated with CCCP, no significant mitochondrial degradation was observed (Figure 5H). Together, these findings indicate a block of global mitophagic flux in *Tsc2*-deficient neurons.

Upon mitochondrial damage, the ubiquitin ligase Parkin is recruited to ubiquitinate mitochondrial proteins. This attracts ubiquitin-binding proteins such as p62, which are believed to facilitate the recruitment of LC3-positive autophagosomes (Figure 4A). Clearance of damaged mitochondria also removes these modifications. Paralleling our studies of mitochondrial flux, we examined the presence of Parkin, ubiquitinated proteins, and LC3 in mitochondrial fractions of *Tsc2*-deficient neurons and controls treated with CCCP (Figures 5I–5K). Polyubiquitinated proteins accumulated in mitochondrial fractions following CCCP treatment with a marked and sustained increase in *Tsc2*-deficient neurons (Figures 5I and 5J). Levels of Parkin and p62 were similarly increased at baseline and remained high following CCCP indicating the continued presence of early mitophagy surrogates in *Tsc2*-deficient neurons (Figures 5I and 5J). Measuring levels of lipidated LC3 (LC3-II), we discovered that it was enriched in mitochondrial fractions of *Tsc2*-deficient neurons both at baseline and after CCCP treatment, reflecting increased amounts of unprocessed autophagosomes (Figures 5I and 5K).

Collectively, these findings demonstrate impaired global mitophagic flux following mitochondrial damage in *Tsc2*-deficient neurons. Our findings point to a block downstream of autophagosome recruitment with proteins involved in early mitophagy and autophagosomes accumulating within mitochondrial fractions of *Tsc2*-deficient neurons.

Deficits in Lysosome-Dependent Stages of Mitophagy

To better understand the block in mitophagic flux downstream of autophagosome recruitment, we analyzed the dynamics of autophagosome formation and recruitment in response to a stimulus that triggers mitophagy. We treated neurons with antimycin A and followed the formation and turnover of LC3-Venus-labeled autophagic vesicles using live-cell confocal imaging (Figure 6A; Movies S4 and S5). At baseline, control cells carry several small LC3-Venus dots or crescent-shaped puncta representing nascent or maturing autophagosomes that are mostly outside of mitochondria-dense areas (Figure 6A). In *Tsc2*-deficient neurons, LC3-Venus is present in fine dot-like vesicles that are observed to partly overlap with mitochondria but also in large vesicular structures that appear in no spatial relationship with mitochondria (Figure 6A). Following induction of mitophagy, control cells rapidly form LC3-positive puncta and show autophagic turnover (Figures 6A–6C). In *Tsc2*-deficient neurons, new LC3-positive vesicles form, but stay relatively small and importantly do not seem to engage in fusion with preexisting large LC3-vesicles, therefore leading to no net increase in mean autophagosome size (Figures 6A–6C). Interestingly, no turnover of newly formed LC3 puncta is appreciated during the course of these live-cell imaging experiments, indicating delayed and/or diminished autophagosome maturation or autophagosome-lysosome fusion in *Tsc2*-deficient cells (Figures 6A and 6B).

To probe autophagosome-lysosome fusion following mitophagy induction, we employed the mCherry-GFP-LC3 tandem

(E and F) Recruitment of lysosomes to axonal mitochondria following acute $\Delta\Psi_m$ depolarization with antimycin A (40 μM). Arrows denote mito-dsRed-labeled mitochondria (red), LysoTracker Green-labeled lysosomes (white), and their co-localization (yellow). Graph shows the maximal percentage of mitochondria co-localizing with lysosomes in individual axons (n > 25 axons per condition from 8 experiments). Scale bar, 5 μm.
AU, arbitrary unit; *p < 0.05, **p < 0.01, ***p < 0.001, ****p < 0.0001. See also Figure S4.

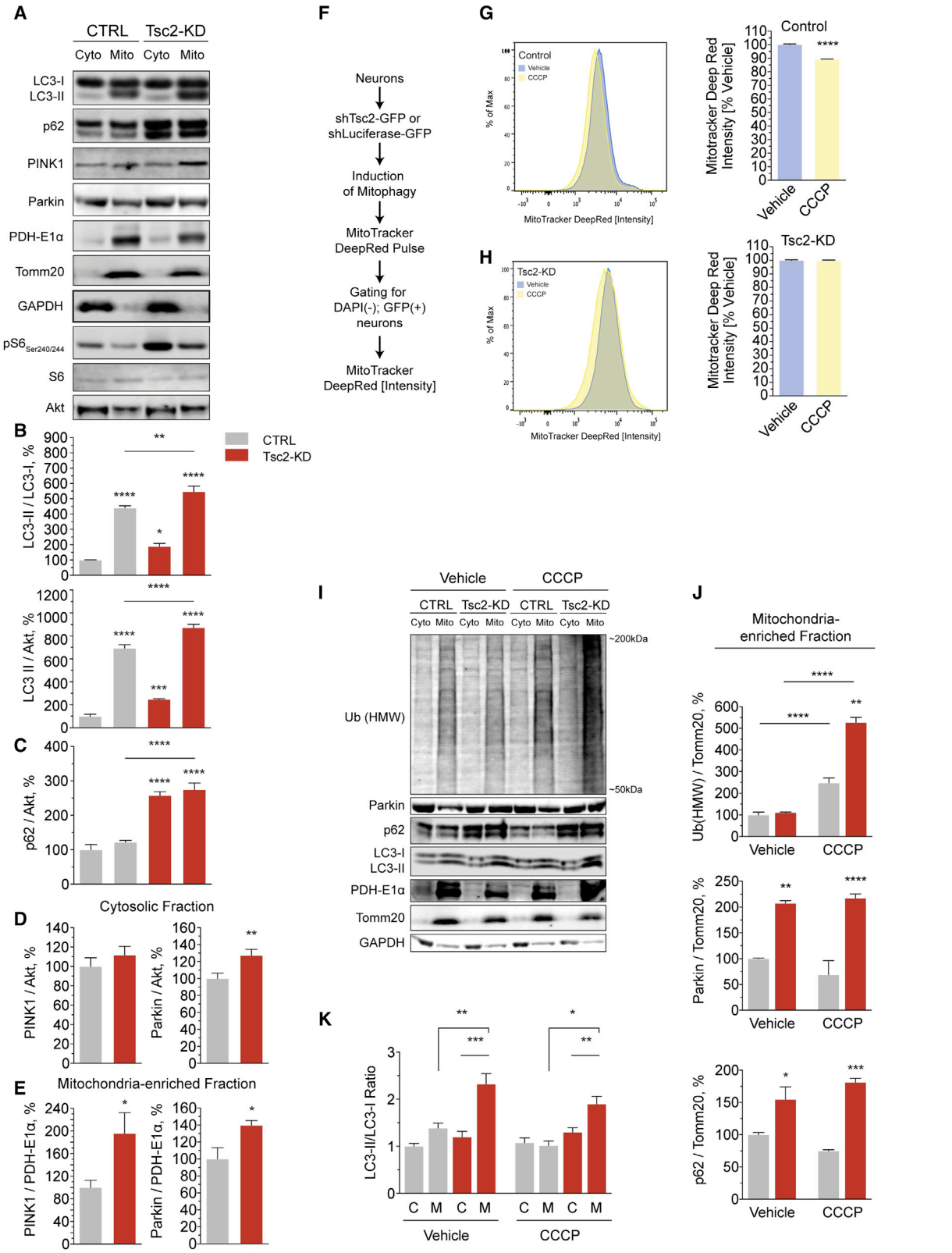

(legend on next page)

assay (Kimura et al., 2007), which allows distinguishing autophagosomes before and after fusion with acidic lysosomes (Figure S5C; Klionsky et al., 2016). Following mitophagy induction, we discovered that nascent autophagosomes mature and to a certain extend are converted to autolysosomes (Figure 6D). In the *Tsc2*-deficient neurons, we did not observe such a recruitment of autolysosomes (Figure 6D). Instead, these vesicles remained at the stage of autophagosomes, further underscoring a block in the late stages of mitochondrial-damage-induced autophagy.

Reduced availability of mature lysosomes may be a rate-limiting factor for autophagosome-lysosome fusion. To quantify the pool of mature lysosomes available for fusion events, we employed an automated confocal microscopy approach to determine the amount of LysoTracker–stained lysosomes in a large number of *Tsc2*-deficient neurons and controls (Figure 6E). Indeed, a smaller area was covered with lysosomal vesicles in *Tsc2*-deficient neurons (Figure 6E), indicating fewer lysosomes available for fusion.

The Impact of mTOR-Dependent and mTOR-Independent Stimulation of Autophagy on Mitochondrial Dynamics, Turnover, and Function

The above experiments demonstrate that mitophagic flux in *Tsc2*-deficient neurons is impaired at the autophagosome recruitment stage and/or downstream lysosome-dependent stages. To test whether mTOR-dependent or mTOR-independent mechanisms are able to overcome or bypass this block in mitophagic flux, we treated neurons with rapamycin (mTORC1 inhibitor, mTOR-dependent enhancer of autophagy; Ravikumar et al., 2002), and carbamazepine (mTOR-independent enhancer of autophagic flux; Maetzel et al., 2014). We found that both treatments engaged the formation of LC3-II and reduced levels of the autophagy substrate p62, confirming that autophagic flux is induced (Figure S6A). Quantifying global mitophagic flux, we discovered that acute inhibition of mTORC1 with rapamycin did not induce a substantial turnover of mitochondria in *Tsc2*-deficient neurons (Figure 7A). Carbamazepine, however, robustly reduced mitochondrial content in *Tsc2*-deficient neurons to about 85% of that of vehicle-treated controls (Figure 7A). Probing the recruitment of autophagosomes to axonal mitochondria, we found that both treatments stimulated the recruitment of LC3-positive autophagosomes to damaged mitochondria (Figure 7B). Interestingly both treatments also increased co-localization of autophagosomes with mitochondria at baseline, without an additional mitophagic stimulus (Figure 7B). This could indicate that existing damaged mitochondria are targeted when autophagic flux is stimulated. In line with the data on global mitophagic flux, carbamazepine showed a particularly strong effect in *Tsc2*-deficient axons (Figure 7B). Combining rapamycin and carbamazepine had no additive effect, suggesting that each treatment alone may achieve saturating levels of autophagy induction in axons.

To test the relevance of these findings for neurons in vivo, we treated $Tsc1^{cc}$;$Syn1Cre^{+}$ mice with rapamycin and prepared mitochondria-enriched fractions from cortex. Mitochondrial fractions of $Tsc1^{cc}$;$Syn1Cre^{+}$ mice accumulate LC3 and p62, both of which were reduced in rapamycin-treated mice (Figures 7C and 7D). Levels of Parkin and of the mitochondrial marker Tomm20 were also reduced following rapamycin treatment, suggesting that $Tsc1^{cc}$;$Syn1Cre^{+}$ mice can effectively prevent or clear mitochondria targeted for mitophagy once mTORC1 signaling is inhibited and autophagic flux is engaged as evidence by an increased cytosolic LC3II/LC3I ratio (Figures 7C and S6B).

Does a correction of axonal mitophagy replenish axons with mitochondria? To address this question, we determined the number of mitochondria per axon area in cultured *Tsc2*-deficient neurons and callosal axons of $Tsc1^{cc}$;$Syn1Cre^{+}$ mice. In vitro, rapamycin and carbamazepine significantly increased the number of axonal mitochondria to levels that either did not differ from or surpassed controls (Figure 7E). In vivo, chronic treatment of $Tsc1^{cc}$;$Syn1Cre^{+}$ mice with rapamycin also normalized the number of mitochondria in callosal axons to levels that are similar to those in control littermates (Figure 7F). In addition to local turnover, influx of new mitochondria from the cell body and mechanisms that promote their peripheral anchoring determine the availability of mitochondria to distal axonal regions. Examining transport patterns of axonal mitochondria, we discovered that rapamycin and carbamazepine promoted the time that these spend in a stationary position at the expense of the increased retrograde transport observed in *Tsc2*-deficient neurons without treatment (Figures 7G–7I). Rapamycin particularly promoted their anterograde transport (Figure 7G), perhaps leading to an even greater replenishment of axonal mitochondria (Figure 7E).

To explore the functional consequences of correcting local mitochondrial turnover and transport, we quantified the capturing of mitochondria at presynaptic sites (Figures 7H and 7I). Although both treatments and their combination did not influence the overall number of presynaptic sites, they led to an increase in the proportion of presynaptic sites that are supported by stationary mitochondria (Figure 7H). Likewise, the dwell time of motile mitochondria at presynaptic sites increased to levels that were similar to those in control axons (Figure 7I). Arguing for an increased anchoring specifically at presynaptic sites, the dwell time outside of presynaptic compartments remained unchanged (Figure 7I).

In summary, these data suggest that suppressing mTORC1 hyperactivity or inducing mTOR-independent autophagy can reverse many of the changes in mitochondrial dynamics and

Figure 5. Global Mitophagic Flux Is Impaired in *Tsc2*-Deficient Neurons

(A–E) Representative western blots and quantification of several proteins involved in mitophagy in cytosolic and mitochondria-enriched fractions from cortical neurons (DIV7/8, n = 12 experiments).

(F–H) Mitophagic flux induced by CCCP (1 μM, 24 hr) quantified using flow cytometry in cortical neurons (DIV11, n = 6 × 10^6 recorded events from 6 experiments).

(I–K) Western blotting for several proteins involved in mitophagy in cytosolic and mitochondria-enriched fractions from cortical neurons (DIV7/8) treated with CCCP (1 μM, 24 hr) or vehicle (n = 3–6 experiments).

C, Cyto, cytosolic fraction; HMW, high molecular weight; M, Mito, mitochondria-enriched fraction; mono, monomeric; *p < 0.05, **p < 0.01, ***p < 0.001, ****p < 0.0001. See also Figure S5.

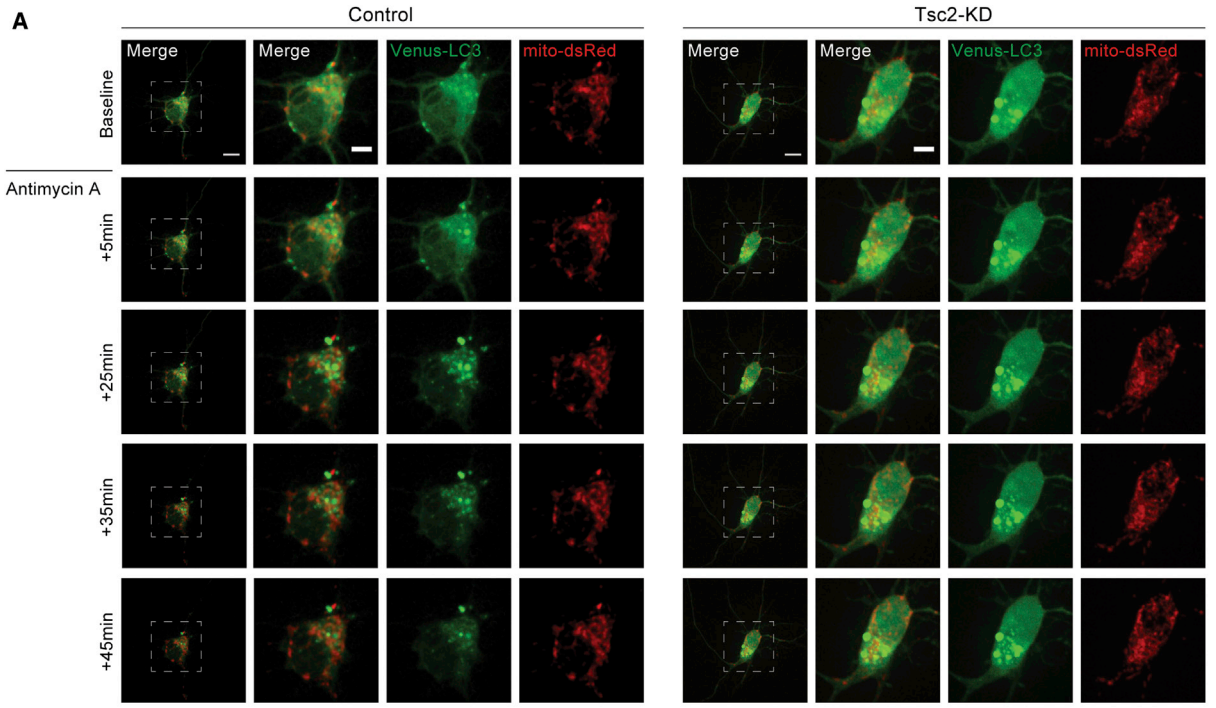

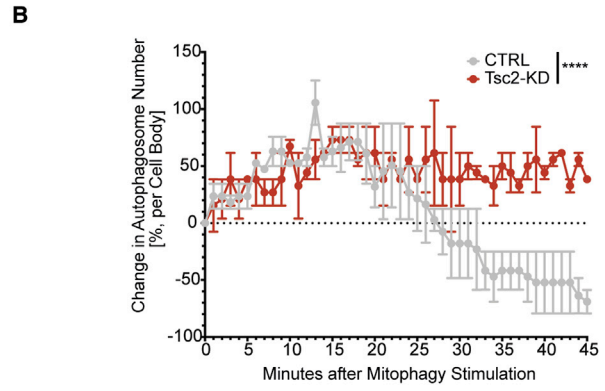

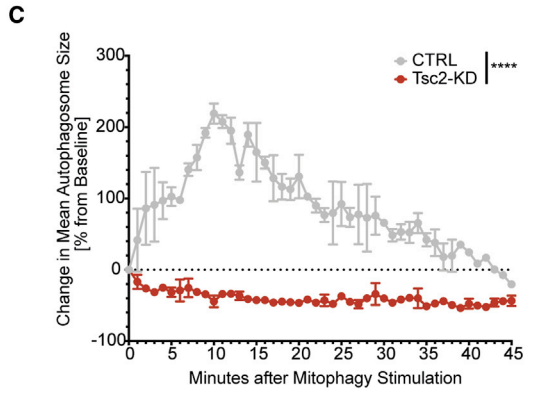

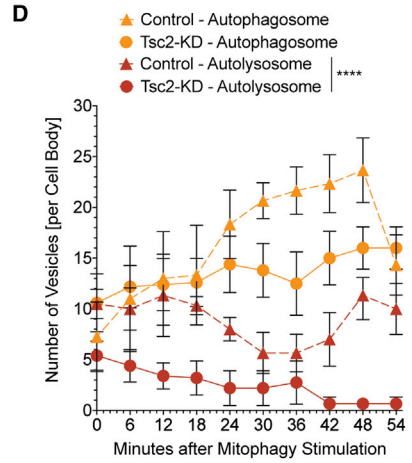

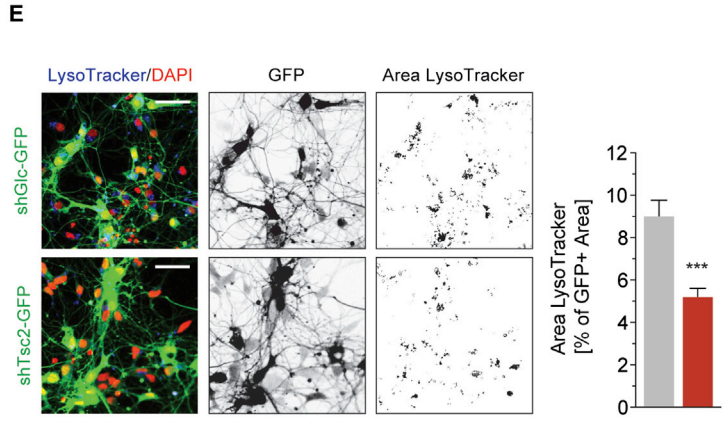

(legend on next page)

turnover seen in *Tsc2*-deficient neurons. Chronic treatment with rapamycin or carbamazepine for 7 days also improved $\Delta\Psi_m$ (Figure S6C), whereas short-term treatment did not (Figure S6D). This dependence on chronic treatment argues that a complete restoration of mitochondrial function is only achieved when several stages of mitochondrial dynamics are intact for a prolonged time period.

DISCUSSION

Mitochondria are critical to many neuronal functions and their dynamics and turnover are tightly regulated. Autophagy is the principal pathway that clears damaged, aged, and superfluous mitochondria (Pickrell and Youle, 2015). Previous work has shown that autophagy is significantly impaired in *TSC*-deficient cells and tissues (Di Nardo et al., 2014; McMahon et al., 2012; Parkhitko et al., 2011; Tang et al., 2014; Yasin et al., 2013). Identifying specific deficits downstream of mTORC1 and autophagy dysfunction may reveal more precise targets for therapeutic interventions. Mitochondria are substrates of autophagy but also essential for mTOR-hyperactivity-induced anabolism; thus, it is important to understand how *TSC* deficiency impacts mitochondrial homeostasis in neurons.

Here, we address this question through a characterization of mitochondrial turnover and dynamics in neuronal in vitro and in vivo models of TSC. Using multiple approaches, we identified deficits in global and local mitophagy in *Tsc2*-deficient neurons and downstream accumulation of mitochondria, with at least a subset of organelles being defective. Importantly, we find that these changes in mitochondrial turnover affect the dynamics and integrity of axonal mitochondria leading to a depletion of functional mitochondria from presynaptic sites.

Mitophagy and Mitochondrial Fragmentation in TSC

The mitochondrial content in any given cell and their maintenance are subject to a complex interplay between mitochondrial biogenesis and degradation. In dividing, non-neuronal cells, loss of *TSC2* leads to an increase in mitochondrial mass (Koyanagi et al., 2011; Morita et al., 2013) that is accompanied by an increase in the transcription of genes associated with mitochondrial biogenesis (Cunningham et al., 2007). In *Tsc2*-deficient neurons, we discovered an increased mitochondrial mass that seems to progress with maturation in vitro but were unable to identify an increase in mRNA levels of the core mitochondrial biogenesis genes, *Pgc1α*, *Nrf-1*, and *mTFAM*. Therefore, increased biogenesis is not likely to drive the increased mitochondrial mass observed in *Tsc2*-deficient neurons.

When mitochondria are excessively abundant, damaged, or aged, mitophagy is engaged to restore homeostasis. Mitophagy undergoes several stages and relies on the general autophagy program to clear mitochondria via engulfment by autophagic vesicles and finally degradation in autolysosomes, the product of mature autophagosomes and lysosomes (Figure 4A). In *Tsc2*-deficient neurons, we discovered a reduction in CCCP-induced mitophagic flux and an accumulation of proteins involved in the early steps of mitophagy, such as PINK1 and Parkin, in mitochondrial preparations. Similarly, we found abundant levels of p62, a stress-induced ubiquitin-binding protein, that, in addition to other functions, may be acting as a selective receptor for targeting damaged mitochondria to autophagosomes (Okatsu et al., 2010) and is commonly found in protein aggregates that result from autophagy impairment (Komatsu et al., 2007). We observed abundant levels of the autophagosome marker LC3-II in mitochondria-enriched fractions of *Tsc2*-deficient neurons, with no significant change after stimulation of mitophagy with CCCP. These results suggest that proteins involved in the early steps of mitophagy accumulate in *Tsc2*-deficient neurons. Although mitophagy is engaged following the introduction of mitochondrial damage, it does not progress to the degradation of mitochondria and no net loss of mitochondria can be detected. Pointing to a block in the late stages of the autophagy pathway, autophagosome maturation into autolysosomes following mitophagy induction was impaired. Levels of lysosomes were reduced in *Tsc2*-deficient neurons, suggesting that the pool of mature lysosomes available for fusion with autophagosomes may be limited.

Mitochondrial morphology mirrors changes in turnover and function and can thus serve as a surrogate for both. Mitochondrial fragmentation is found in many forms of mtDNA diseases with reduced oxidative phosphorylation, where it is thought to segregate mitochondria containing deleterious mutations and may promote their degradation through autophagy (Pryde et al., 2016; Twig et al., 2008). In *Tsc1/2*-deficient neurons, we discovered a reduction of the average size of axonal mitochondria both in vitro and in vivo. We further found an increase in the circularity of axonal mitochondria, pointing to ongoing mitochondrial fragmentation reflecting dysfunction and perhaps ensuing turnover.

Axonal and Presynaptic Mitochondria in TSC

Intellectual disability, seizures, and autism spectrum disorder in many patients with TSC may at least in part originate from synaptic dysfunction (Sahin and Sur, 2015). Underscoring the importance of axonal mitochondria in this process, removing mitochondria from axon terminals has been shown to result in aberrant synaptic transmission (Ma et al., 2009; Verstreken et al., 2005). Mitochondrial dysfunction, reactive oxygen species, and a reduced availability of functional mitochondria

Figure 6. Deficits in the Lysosome-Dependent Stages of Mitophagy in *Tsc2*-Deficient Neurons

(A–C) Autophagosome turnover in hippocampal neurons (DIV7/8) acutely treated with antimycin A (40 μM). Graphs show the percent change in autophagosome number and size from baseline (n = 3 experiments). Scale bar, 10 μm, 5 μm (inset).

(D) Autophagosomes (GFP+ and mCherry+) and autolysosomes (RFP+only) in hippocampal neurons (DIV7/8) transfected with mCherry-EGFP-LC3 and acutely treated with antimycin A (40 μM; n = 4 experiments).

(E) LysoTracker Deep Red-stained lysosomes in hippocampal neurons (DIV7/8). Graph shows the lysosomal area as a percentage of the GFP-stained cell area (n > 25 × 10^3 cells per condition from 3 experiments). Scale bar, 40 μm.

***p < 0.001, ****p < 0.0001. See also Figure S5.

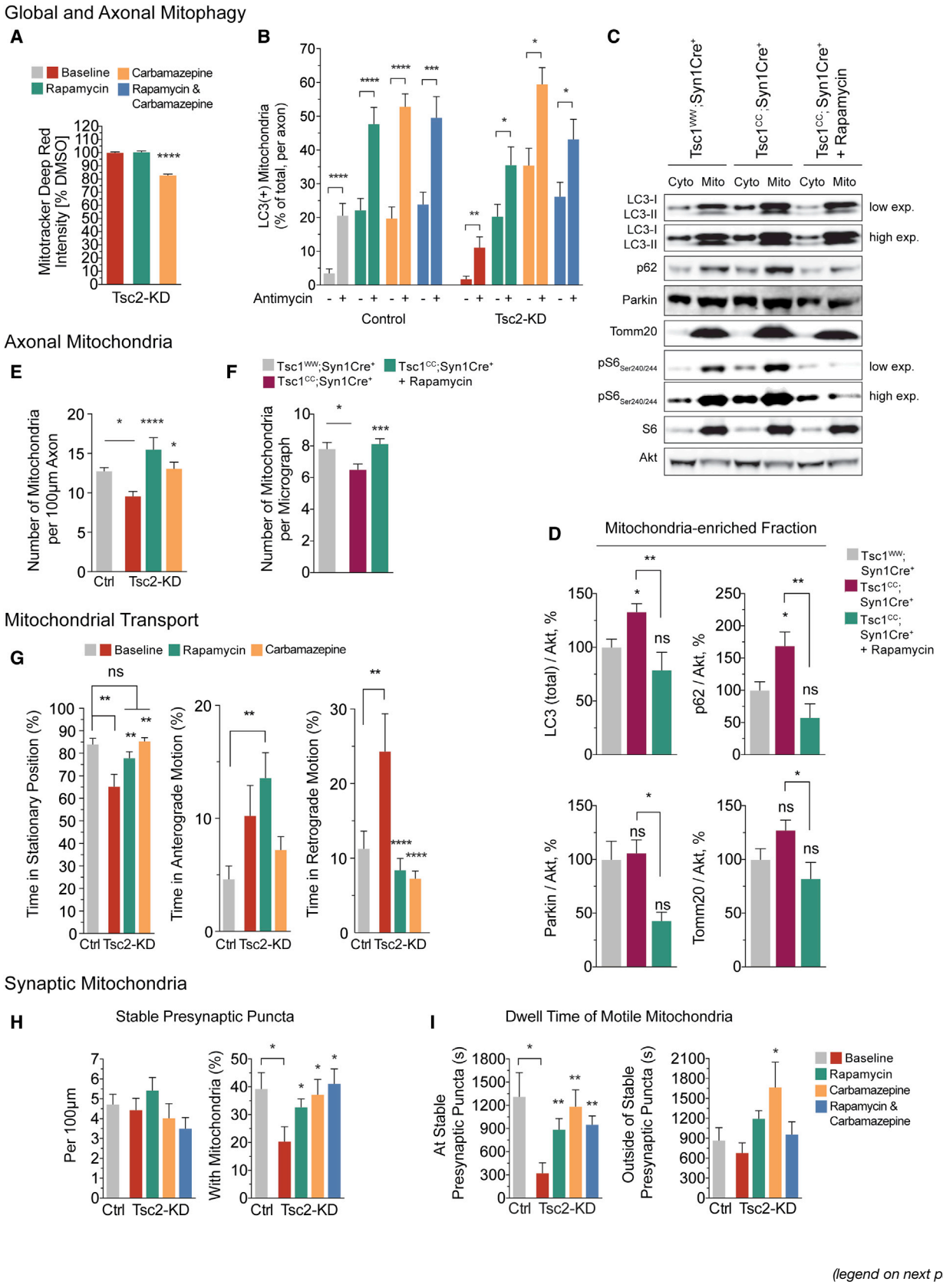

(legend on next page)

to synapses, as a result of impaired mitophagy, may critically impair synaptic function (Haddad et al., 2013; Santini et al., 2015).

Axonal mitochondria are subject to active transportation (Sheng, 2014) and local turnover (Ashrafi et al., 2014). We explored both in *Tsc2*-deficient neurons. Mitochondria were relatively depleted from *Tsc2*-deficient axons, which may be partly explained by an increased retrograde transportation of mostly damaged mitochondria. Damaged mitochondria were frequently observed and may be a result of impaired local turnover through mitophagy. In light of these findings, we speculate that reduced axonal mitophagy may lead to a buildup of damaged mitochondria over time. This buildup is met with increased retrograde transportation to clear dysfunctional and potentially harmful organelles from vulnerable, distal regions and perhaps leads to their clustering in the cell body where lysosomes are relatively enriched. The net effect of this is a depletion of axonal mitochondria.

Because of great regional differences in demand for ATP supply and calcium buffering, axonal mitochondria are transported bidirectionally and anchored as needed, particularly at active sites such as synapses (Rangaraju et al., 2014). To probe the availability of mitochondria to synapses, we investigated presynaptic capturing of mitochondria in developing and more mature axons. We discovered that presynaptic sites in *Tsc2*-deficient neurons were deprived of stationary mitochondria. In addition, we found that motile mitochondria, known to provide their function to presynaptic compartments en passant, spend less time dwelling over presynaptic sites. The reduced availability of mitochondria at synapses may bear importance to altered neuronal connectivity, intellectual disability, and seizures in TSC.

Correcting Deficits in Mitochondrial Homeostasis in TSC

mTOR inhibitors have been shown to correct many molecular and behavioral deficits in neuronal models of TSC. This has paved the way for randomized placebo-controlled trials of mTOR inhibitors for neurocognitive deficits in children with TSC (Ebrahimi-Fakhari and Sahin, 2015). Autophagy can be activated in an mTORC1-dependent manner or by mechanisms that do not rely on mTOR kinase activity (Ebrahimi-Fakhari et al., 2014, 2016). To assess whether enhancing autophagy could correct mitochondrial deficits in *Tsc2*-deficient neurons, we treated them with rapamycin and carbamazepine. The latter is a widely used anticonvulsive drug that is thought to engage autophagy through reducing free inositol and myoinositiol-1,4,5-triphosphate levels (Sarkar et al., 2005; Schiebler et al., 2014). Both treatments corrected multiple deficits and importantly replenished axonal mitochondria, including those that support presynaptic sites. Our data thus indicate that induction of autophagy itself is beneficial and suggest that both compounds can restore the clearance of damaged mitochondria. This also implies that, once autophagy deficits are bypassed, lysosomal proteolysis is functional in *Tsc2*-deficient neurons. These experiments also indicate that the deficits in lysosome-dependent stages of mitophagy still enable some increased substrate flux upon induction of autophagosome biogenesis, suggesting that the principal defect in mitochondrial turnover in *Tsc2*-deficient neurons results from a compromise of the autophagy-lysosomal pathway and is not primarily caused by impairment of early mitophagy events such as PINK1 or Parkin signaling. The fact that combining both treatments did not have an additive effect suggests that autophagy, rather than other downstream targets of mTORC1 signaling, is likely the main contributor to the restoration of mitochondrial phenotypes in *Tsc2*-deficient neurons, with either treatment alone achieving saturated levels of autophagy induction.

Our findings lend support to the concept that promoting clearance of damaged mitochondria through engaging autophagic flux by mTOR-dependent and -independent mechanisms has potential therapeutic value for neurological diseases with mitochondrial dysfunction. Along these lines, rapamycin has been successfully used to drive selection against pathogenic mtDNA mutations in models of mtDNA diseases (Dai et al., 2014; Johnson et al., 2013). We acknowledge, however, that even though we probe mTORC1-dependent and independent mechanisms to bypass autophagy deficits, future studies will need to fully dissect the role of mTORC1 inhibition in restoring mitochondrial deficits beyond correction of mitochondrial turnover (Johnson

Figure 7. The Impact of mTOR-Dependent and mTOR-Independent Stimulation of Autophagy on Mitochondrial Dynamics, Turnover, and Function

(A) Quantification of mitophagic flux using flow cytometry in cortical neurons (DIV11) treated with rapamycin (20 nM, 24 hr) or carbamazepine (100 μM, 24 hr, n = 3 × 10^6 recorded events per condition from 3–6 experiments).

(B) Recruitment of Venus-LC3-labeled autophagosomes to axonal mitochondria following acute $\Delta\Psi_m$ depolarization with antimycin A (40 μM) in hippocampal neurons (DIV7/8) pretreated with rapamycin, carbamazepine, or a combination of both drugs (n > 35 axons per condition from 5–10 experiments).

(C and D) Western blotting for several proteins involved in mitophagy in cytosolic and mitochondria-enriched fractions from cortex of *Tsc1^{cc};Syn1Cre^{+}* mice (n = 8), *Tsc1^{CC};Syn1Cre^{+}* mice treated with rapamycin (n = 4), and *Tsc1^{ww};Syn1Cre^{+}* littermates (n = 8, post-natal day [P]21).

(E) Number of mitochondria per 100-μm axon in hippocampal neurons (DIV 7/8) pretreated with rapamycin or carbamazepine (n > 20 axons per condition from >4 experiments).

(F) Number of mitochondria in callosal projection axons from *Tsc1^{cc};Syn1Cre^{+}* mice (n = 2), *Tsc1^{cc};Syn1Cre^{+}* mice treated with rapamycin (n = 3), and *Tsc1^{ww};Syn1Cre^{+}* littermate controls (n = 3, P21) using transmission electron microscopy.

(G) Mitochondrial transport in the mid-axon of hippocampal neurons (DIV7/8) pretreated with rapamycin or carbamazepine (n > 15 axons per condition from 3–5 experiments).

(H) Number of stable presynaptic puncta per 100-μm axon and the percentage of stable presynaptic puncta supported by mitochondria in hippocampal neurons (DIV7/8) pretreated with rapamycin (20 nM, 24 hr), carbamazepine (100 μM, 24 hr), or a combination of both drugs (n = 14 axons per condition from 7 experiments).

(I) Dwell time of motile mitochondria at and outside of stable presynaptic puncta in hippocampal neurons (DIV7/8) pretreated with rapamycin, carbamazepine, or a combination of both drugs (n = 14 axons per condition from 7 experiments).

Cyto, cytosolic fraction; Mito, mitochondrial fraction; ns, not significant; *p < 0.05, **p < 0.01, ***p < 0.001, ****p < 0.0001. See also Figure S6.

et al., 2013; Zheng et al., 2016). Likewise, the mechanisms by which deficits in the lysosome-dependent stages of mitophagy are bypassed or corrected upon increased autophagic flux remain to be investigated in detail.

In summary, our results provide evidence for a role of impaired neuronal mitophagy in TSC, by showing that mTORC1 hyperactivity impairs the lysosome-dependent stages of mitochondrial turnover. Our study clarifies the complex relationship between the TSC-mTORC1 pathway, autophagy, and mitophagy, and defines mitochondrial homeostasis as a therapeutic target for TSC and related diseases.

EXPERIMENTAL PROCEDURES

Please see the Supplemental Experimental Procedures for details.

Animals

Tsc1^{cc}*;Syn1Cre*$^{+}$ mice were described previously (Meikle et al., 2007). Rapamycin was administered i.p. at 6 mg/kg every other day starting at postnatal day 7.

Generation of Human iPSC and Cortical Neuron Differentiation

Human iPSCs were generated using episomal plasmids to introduce the reprogramming factors (Oct4, Sox2, Klf4, and L-Myc) into blood cells or fibroblasts (Table S1). Homozygous *TSC2* mutant iPSC lines were generated using TALEN-mediated mutagenesis. Cortical neuronal differentiation was adapted from Zhang et al. (2013).

Live-Cell Confocal Imaging

Confocal images were obtained using a spinning disk confocal microscope (Perkin Elmer) with a Nikon Ti-Eclipse live cell imaging system and Volocity software (Perkin Elmer).

Mitochondrial Motility

A mid-axonal compartment (~500–800 μm from the soma) was identified, and images were captured every 3 s. Individual mitochondria were analyzed in a standardized manner using the custom-written Kymolizer macro in ImageJ (Pekkurnaz et al., 2014).

Axonal Mitophagy

LC3 and lysosome recruitment to mitochondria was quantified as described in Ashrafi et al. (2014).

Presynaptic Capturing of Mitochondria

Mitochondrial capturing at synapses was measured as described in Courchet et al. (2013).

Statistical Analysis

Statistical analysis was performed with GraphPad Prism 6.0 (GraphPad Software). Throughout the manuscript, the distribution of data points is expressed as mean ± SEM. Mann-Whitney U test, unpaired Student t test or one-way ANOVA with post hoc Bonferroni's multiple-comparisons test was used to determine significance. $p < 0.05$ was considered significant.

SUPPLEMENTAL INFORMATION

Supplemental Information includes Supplemental Experimental Procedures, six figures, one table, and five movies and can be found with this article online at http://dx.doi.org/10.1016/j.celrep.2016.09.054.

AUTHOR CONTRIBUTIONS

D.E.-F., A.S., L.W., and M.S. conceived and designed the experiments. D.E.-F., A.S., L.W., A.D., D.T., C.C., J.M.R., and M-J.H. performed the experiments. D.E.-F., A.S., L.W., A.D., C.C., J.M.R., M-J.H., and M.S. analyzed the data. S.K., G.F.H., T.L.L., J.O.L., and F.P. contributed reagents/materials/analysis tools. D.E.-F., A.S., and M.S. drafted the article. D.E.-F., A.S., L.W., A.D., D.T., T.L.L., C.C., J.M.R., J.O.L., S.K., G.F.H., M.-J.H., F.P., and M.S. revised the article.

ACKNOWLEDGMENTS

We thank R. Kleiman, J. Micozzi, X. Yang, E. Ercan, E. Chadwick, S. Lammers, S. Schaeffer, C. Super (Boston Children's Hospital [BCH]), and D.J. Kwiatkowski (Brigham and Women's Hospital) for helpful discussions and technical assistance. We are also grateful to A. Hill and the IDDRC Cellular Imaging Core (funded by NIH P30HD18655) at BCH for technical support and to G. Ashrafi, G. Pekkurnaz, and T.L. Schwarz (BCH) for sharing reagents, software and advice. This work was supported by the Graduate Academy (D.E.-F.) and the Young Investigator Award Program at Heidelberg University (grant F.206773) (D.E.-F. and L.W.), the Daimler & Benz Foundation (grant 32-05/13) (D.E.-F.), the Reinhard-Frank Foundation (D.E.-F.), the German National Academic Foundation (A.S.), the Nancy Lurie Marks Family Foundation, and the Boston Children's Hospital Translational Research Program (M.S.). C.C. and J.M.R. are affiliated with LAM Therapeutics. Other research projects in the Sahin Laboratory are affiliated with Novartis and Pfizer.

Received: April 22, 2016
Revised: July 11, 2016
Accepted: September 15, 2016
Published: October 18, 2016

REFERENCES

Albert, V., and Hall, M.N. (2015). mTOR signaling in cellular and organismal energetics. Curr. Opin. Cell Biol. *33*, 55–66.

Ashrafi, G., Schlehe, J.S., LaVoie, M.J., and Schwarz, T.L. (2014). Mitophagy of damaged mitochondria occurs locally in distal neuronal axons and requires PINK1 and Parkin. J. Cell Biol. *206*, 655–670.

Cai, Q., Zakaria, H.M., Simone, A., and Sheng, Z.H. (2012). Spatial parkin translocation and degradation of damaged mitochondria via mitophagy in live cortical neurons. Curr. Biol. *22*, 545–552.

Choi, Y.J., Di Nardo, A., Kramvis, I., Meikle, L., Kwiatkowski, D.J., Sahin, M., and He, X. (2008). Tuberous sclerosis complex proteins control axon formation. Genes Dev. *22*, 2485–2495.

Costa, V., Aigner, S., Vukcevic, M., Sauter, E., Behr, K., Ebeling, M., Dunkley, T., Friedlein, A., Zoffmann, S., Meyer, C.A., et al. (2016). mTORC1 inhibition corrects neurodevelopmental and synaptic alterations in a human stem cell model of tuberous sclerosis. Cell Rep. *15*, 86–95.

Courchet, J., Lewis, T.L., Jr., Lee, S., Courchet, V., Liou, D.Y., Aizawa, S., and Polleux, F. (2013). Terminal axon branching is regulated by the LKB1-NUAK1 kinase pathway via presynaptic mitochondrial capture. Cell *153*, 1510–1525.

Cunningham, J.T., Rodgers, J.T., Arlow, D.H., Vazquez, F., Mootha, V.K., and Puigserver, P. (2007). mTOR controls mitochondrial oxidative function through a YY1-PGC-1alpha transcriptional complex. Nature *450*, 736–740.

Dai, Y., Zheng, K., Clark, J., Swerdlow, R.H., Pulst, S.M., Sutton, J.P., Shinobu, L.A., and Simon, D.K. (2014). Rapamycin drives selection against a pathogenic heteroplasmic mitochondrial DNA mutation. Hum. Mol. Genet. *23*, 637–647.

Devireddy, S., Liu, A., Lampe, T., and Hollenbeck, P.J. (2015). The organization of mitochondrial quality control and life cycle in the nervous system in vivo in the absence of PINK1. J. Neurosci. *35*, 9391–9401.

Di Nardo, A., Kramvis, I., Cho, N., Sadowski, A., Meikle, L., Kwiatkowski, D.J., and Sahin, M. (2009). Tuberous sclerosis complex activity is required to control neuronal stress responses in an mTOR-dependent manner. J. Neurosci. *29*, 5926–5937.

Di Nardo, A., Wertz, M.H., Kwiatkowski, E., Tsai, P.T., Leech, J.D., Greene-Colozzi, E., Goto, J., Dilsiz, P., Talos, D.M., Clish, C.B., et al. (2014). Neuronal Tsc1/2 complex controls autophagy through AMPK-dependent regulation of ULK1. Hum. Mol. Genet. *23*, 3865–3874.

DiMario, F.J., Jr., Sahin, M., and Ebrahimi-Fakhari, D. (2015). Tuberous sclerosis complex. Pediatr. Clin. North Am. *62*, 633–648.

Ebrahimi-Fakhari, D., and Sahin, M. (2015). Autism and the synapse: emerging mechanisms and mechanism-based therapies. Curr. Opin. Neurol. *28*, 91–102.

Ebrahimi-Fakhari, D., Wahlster, L., Hoffmann, G.F., and Kölker, S. (2014). Emerging role of autophagy in pediatric neurodegenerative and neurometabolic diseases. Pediatr. Res. *75*, 217–226.

Ebrahimi-Fakhari, D., Saffari, A., Wahlster, L., Lu, J., Byrne, S., Hoffmann, G.F., Jungbluth, H., and Sahin, M. (2016). Congenital disorders of autophagy: an emerging novel class of inborn errors of neuro-metabolism. Brain *139*, 317–337.

Goto, J., Talos, D.M., Klein, P., Qin, W., Chekaluk, Y.I., Anderl, S., Malinowska, I.A., Di Nardo, A., Bronson, R.T., Chan, J.A., et al. (2011). Regulable neural progenitor-specific Tsc1 loss yields giant cells with organellar dysfunction in a model of tuberous sclerosis complex. Proc. Natl. Acad. Sci. USA *108*, E1070–E1079.

Haddad, D.M., Vilain, S., Vos, M., Esposito, G., Matta, S., Kalscheuer, V.M., Craessaerts, K., Leyssen, M., Nascimento, R.M., Vianna-Morgante, A.M., et al. (2013). Mutations in the intellectual disability gene Ube2a cause neuronal dysfunction and impair parkin-dependent mitophagy. Mol. Cell *50*, 831–843.

Johnson, S.C., Yanos, M.E., Kayser, E.B., Quintana, A., Sangesland, M., Castanza, A., Uhde, L., Hui, J., Wall, V.Z., Gagnidze, A., et al. (2013). mTOR inhibition alleviates mitochondrial disease in a mouse model of Leigh syndrome. Science *342*, 1524–1528.

Johnson, D.E., Ostrowski, P., Jaumouillé, V., and Grinstein, S. (2016). The position of lysosomes within the cell determines their luminal pH. J. Cell Biol. *212*, 677–692.

Kimura, S., Noda, T., and Yoshimori, T. (2007). Dissection of the autophagosome maturation process by a novel reporter protein, tandem fluorescent-tagged LC3. Autophagy *3*, 452–460.

Klionsky, D.J., Abdelmohsen, K., Abe, A., Abedin, M.J., Abeliovich, H., Acevedo Arozena, A., Adachi, H., Adams, C.M., Adams, P.D., Adeli, K., et al. (2016). Guidelines for the use and interpretation of assays for monitoring autophagy (3rd edition). Autophagy *12*, 1–222.

Komatsu, M., Waguri, S., Koike, M., Sou, Y.S., Ueno, T., Hara, T., Mizushima, N., Iwata, J., Ezaki, J., Murata, S., et al. (2007). Homeostatic levels of p62 control cytoplasmic inclusion body formation in autophagy-deficient mice. Cell *131*, 1149–1163.

Koyanagi, M., Asahara, S., Matsuda, T., Hashimoto, N., Shigeyama, Y., Shibutani, Y., Kanno, A., Fuchita, M., Mikami, T., Hosooka, T., et al. (2011). Ablation of TSC2 enhances insulin secretion by increasing the number of mitochondria through activation of mTORC1. PLoS One *6*, e23238.

Lipton, J.O., and Sahin, M. (2014). The neurology of mTOR. Neuron *84*, 275–291.

Ma, H., Cai, Q., Lu, W., Sheng, Z.H., and Mochida, S. (2009). KIF5B motor adaptor syntabulin maintains synaptic transmission in sympathetic neurons. J. Neurosci. *29*, 13019–13029.

Maday, S., Twelvetrees, A.E., Moughamian, A.J., and Holzbaur, E.L. (2014). Axonal transport: cargo-specific mechanisms of motility and regulation. Neuron *84*, 292–309.

Maetzel, D., Sarkar, S., Wang, H., Abi-Mosleh, L., Xu, P., Cheng, A.W., Gao, Q., Mitalipova, M., and Jaenisch, R. (2014). Genetic and chemical correction of cholesterol accumulation and impaired autophagy in hepatic and neural cells derived from Niemann-Pick type C patient-specific iPS cells. Stem Cell Reports *2*, 866–880.

Mauro-Lizcano, M., Esteban-Martínez, L., Seco, E., Serrano-Puebla, A., Garcia-Ledo, L., Figueiredo-Pereira, C., Vieira, H.L., and Boya, P. (2015). New method to assess mitophagy flux by flow cytometry. Autophagy *11*, 833–843.

McMahon, J., Huang, X., Yang, J., Komatsu, M., Yue, Z., Qian, J., Zhu, X., and Huang, Y. (2012). Impaired autophagy in neurons after disinhibition of mammalian target of rapamycin and its contribution to epileptogenesis. J. Neurosci. *32*, 15704–15714.

Meikle, L., Talos, D.M., Onda, H., Pollizzi, K., Rotenberg, A., Sahin, M., Jensen, F.E., and Kwiatkowski, D.J. (2007). A mouse model of tuberous sclerosis: neuronal loss of Tsc1 causes dysplastic and ectopic neurons, reduced myelination, seizure activity, and limited survival. J. Neurosci. *27*, 5546–5558.

Morita, M., Gravel, S.P., Chénard, V., Sikström, K., Zheng, L., Alain, T., Gandin, V., Avizonis, D., Arguello, M., Zakaria, C., et al. (2013). mTORC1 controls mitochondrial activity and biogenesis through 4E-BP-dependent translational regulation. Cell Metab. *18*, 698–711.

Murphy, M.P. (2009). How mitochondria produce reactive oxygen species. Biochem. J. *417*, 1–13.

Narendra, D.P., Jin, S.M., Tanaka, A., Suen, D.F., Gautier, C.A., Shen, J., Cookson, M.R., and Youle, R.J. (2010). PINK1 is selectively stabilized on impaired mitochondria to activate Parkin. PLoS Biol. *8*, e1000298.

Okatsu, K., Saisho, K., Shimanuki, M., Nakada, K., Shitara, H., Sou, Y.S., Kimura, M., Sato, S., Hattori, N., Komatsu, M., et al. (2010). p62/SQSTM1 cooperates with Parkin for perinuclear clustering of depolarized mitochondria. Genes Cells *15*, 887–900.

Parkhitko, A., Myachina, F., Morrison, T.A., Hindi, K.M., Auricchio, N., Karbowniczek, M., Wu, J.J., Finkel, T., Kwiatkowski, D.J., Yu, J.J., and Henske, E.P. (2011). Tumorigenesis in tuberous sclerosis complex is autophagy and p62/sequestosome 1 (SQSTM1)-dependent. Proc. Natl. Acad. Sci. USA *108*, 12455–12460.

Pekkurnaz, G., Trinidad, J.C., Wang, X., Kong, D., and Schwarz, T.L. (2014). Glucose regulates mitochondrial motility via Milton modification by O-GlcNAc transferase. Cell *158*, 54–68.

Pernas, L., and Scorrano, L. (2016). Mito-morphosis: Mitochondrial fusion, fission, and cristae remodeling as key mediators of cellular function. Annu. Rev. Physiol. *78*, 505–531.

Pickrell, A.M., and Youle, R.J. (2015). The roles of PINK1, parkin, and mitochondrial fidelity in Parkinson's disease. Neuron *85*, 257–273.

Pryde, K.R., Smith, H.L., Chau, K.-Y., and Schapira, A.H.V. (2016). PINK1 disables the anti-fission machinery to segregate damaged mitochondria for mitophagy. J. Cell Biol. *213*, 163–171.

Rangaraju, V., Calloway, N., and Ryan, T.A. (2014). Activity-driven local ATP synthesis is required for synaptic function. Cell *156*, 825–835.

Ravikumar, B., Duden, R., and Rubinsztein, D.C. (2002). Aggregate-prone proteins with polyglutamine and polyalanine expansions are degraded by autophagy. Hum. Mol. Genet. *11*, 1107–1117.

Sahin, M., and Sur, M. (2015). Genes, circuits, and precision therapies for autism and related neurodevelopmental disorders. Science *350*, aab3897.

Santini, E., Turner, K.L., Ramaraj, A.B., Murphy, M.P., Klann, E., and Kaphzan, H. (2015). Mitochondrial superoxide contributes to hippocampal synaptic dysfunction and memory deficits in angelman syndrome model mice. J. Neurosci. *35*, 16213–16220.

Sarkar, S., Floto, R.A., Berger, Z., Imarisio, S., Cordenier, A., Pasco, M., Cook, L.J., and Rubinsztein, D.C. (2005). Lithium induces autophagy by inhibiting inositol monophosphatase. J. Cell Biol. *170*, 1101–1111.

Schiebler, M., Brown, K., Hegyi, K., Newton, S.M., Renna, M., Hepburn, L., Klapholz, C., Coulter, S., Obregón-Henao, A., Henao Tamayo, M., et al. (2014). Functional drug screening reveals anticonvulsants as enhancers of mTOR-independent autophagic killing of *Mycobacterium tuberculosis* through inositol depletion. EMBO Mol. Med. *7*, 127–139.

Sheng, Z.H. (2014). Mitochondrial trafficking and anchoring in neurons: New insight and implications. J. Cell Biol. *204*, 1087–1098.

Sun, T., Qiao, H., Pan, P.Y., Chen, Y., and Sheng, Z.H. (2013). Motile axonal mitochondria contribute to the variability of presynaptic strength. Cell Rep. *4*, 413–419.

Tang, G., Gudsnuk, K., Kuo, S.H., Cotrina, M.L., Rosoklija, G., Sosunov, A., Sonders, M.S., Kanter, E., Castagna, C., Yamamoto, A., et al. (2014). Loss of mTOR-dependent macroautophagy causes autistic-like synaptic pruning deficits. Neuron *83*, 1131–1143.

Tsai, P.T., Hull, C., Chu, Y., Greene-Colozzi, E., Sadowski, A.R., Leech, J.M., Steinberg, J., Crawley, J.N., Regehr, W.G., and Sahin, M. (2012). Autistic-like behaviour and cerebellar dysfunction in Purkinje cell Tsc1 mutant mice. Nature *488*, 647–651.

Twig, G., Elorza, A., Molina, A.J., Mohamed, H., Wikstrom, J.D., Walzer, G., Stiles, L., Haigh, S.E., Katz, S., Las, G., et al. (2008). Fission and selective fusion govern mitochondrial segregation and elimination by autophagy. EMBO J. *27*, 433–446.

Verstreken, P., Ly, C.V., Venken, K.J., Koh, T.W., Zhou, Y., and Bellen, H.J. (2005). Synaptic mitochondria are critical for mobilization of reserve pool vesicles at *Drosophila* neuromuscular junctions. Neuron *47*, 365–378.

Wang, X., and Schwarz, T.L. (2009). The mechanism of Ca^{2+}-dependent regulation of kinesin-mediated mitochondrial motility. Cell *136*, 163–174.

Wang, X., Winter, D., Ashrafi, G., Schlehe, J., Wong, Y.L., Selkoe, D., Rice, S., Steen, J., LaVoie, M.J., and Schwarz, T.L. (2011). PINK1 and Parkin target Miro for phosphorylation and degradation to arrest mitochondrial motility. Cell *147*, 893–906.

Yasin, S.A., Ali, A.M., Tata, M., Picker, S.R., Anderson, G.W., Latimer-Bowman, E., Nicholson, S.L., Harkness, W., Cross, J.H., Paine, S.M., and Jacques, T.S. (2013). mTOR-dependent abnormalities in autophagy characterize human malformations of cortical development: evidence from focal cortical dysplasia and tuberous sclerosis. Acta Neuropathol. *126*, 207–218.

Zhang, Y., Pak, C., Han, Y., Ahlenius, H., Zhang, Z., Chanda, S., Marro, S., Patzke, C., Acuna, C., Covy, J., et al. (2013). Rapid single-step induction of functional neurons from human pluripotent stem cells. Neuron *78*, 785–798.

Zheng, X., Boyer, L., Jin, M., Kim, Y., Fan, W., Bardy, C., Berggren, T., Evans, R.M., Gage, F.H., and Hunter, T. (2016). Alleviation of neuronal energy deficiency by mTOR inhibition as a treatment for mitochondria-related neurodegeneration. eLife *5*, e13378.